Quasiguided modes of opaline photonic crystals covered by $Ge_2Sb_2Te_5$

S. A. Dyakov[*] and N. A. Gippius

Skolkovo Institute of Science and Technology, 143025 Moscow Region, Russia

M. M. Voronov, S. A. Yakovlev, and A. B. Pevtsov

Ioffe Physical-Technical Institute of the Russian Academy of Sciences, St. Petersburg 194021, Russia

I. A. Akimov

Experimentelle Physik 2, Technische Universität Dortmund, 44221 Dortmund, Germany

S. G. Tikhodeev

A. M. Prokhorov General Physics Institute, RAS, Vavilova 38, Moscow, Russia
and Faculty of Physics, M. V. Lomonosov Moscow State University, 119991 Moscow, Russia

The physical origin of resonant Wood's anomalies in the reflection spectra of three-dimensional (3D) opaline photonic crystals covered with $Ge_2Sb_2Te_5$ (GST225) is discussed. For this purpose, the optical reflection spectra are studied for different incident angles of light both experimentally and theoretically. The performed eigenmode analysis reveals that the Wood's anomalies originate from the quasiguided modes which appear in the GST225 capping layer. This conclusion is supported by the simulated electromagnetic near-field distributions of incident light at resonant frequencies. The experimental reflection spectra are in good agreement with theoretical calculations performed by the Fourier modal method in the scattering matrix form.

I. INTRODUCTION

Opal-based materials have attracted a great deal of attention from researchers over several decades due to their unique properties, ease of fabrication, and high potential for a large variety of applications. The optical properties of opals are strongly determined by the lattice configuration including its period, refractive index, and orientation. Opals having photonic stop bands in the visible range demonstrate shimmered interference colors. This fact not only provokes interest in opals from the viewpoint of jewelry but makes them promising for colorimetric sensors [1,2], solar cells [3–5], and microdisplays [6–8].

The optical properties of opals can be effectively tuned by mechanical deformation of the photonic crystal lattice [8] or by applying electrokinetic force for reshaping the opaline particles [6]. Another way to change the optical properties of the opal is to control the geometry and composition of its surface. Observation of surface states in pure 3D photonic crystals, without any specifically designed termination, was described in the literature both in dielectric [9] and in plasmonic crystals [10]. As was demonstrated in Ref. [11], the presence of gold film terminating the opaline photonic crystal lattice leads to modification of the angular transmission diagram owing to the coupling of the diffracted light to surface plasmon polaritons. In Ref. [12] it was shown that the unstructured silicon interfacial layer between the air and two-dimensional photonic crystal can give rise to Tamm-like surface states that modify the optical reflection of such structure in the spectral region of the photonic stop band.

Very recently, the optical Tamm states were demonstrated in transmission and reflectance spectra of three-dimensional opal photonic crystals coated by thin metal films [13]. These Tamm states provide the bypass for light at the edges of the Bragg diffraction resonances and reduce the diffraction efficiency. Besides that, the configuration of the opal surface was demonstrated to play an important role in second harmonic generation [14] and point imaging by opal slabs with negative refraction [15].

The authors of Refs. [16,17] described the optical properties of opal-based structures impregnated or covered with materials which undergo a phase transition. The reflection spectra of such structures were considered in terms of resonant Wood's anomalies and 3D Bragg diffraction. In Ref. [17], the phenomenological theory was developed based on the Laue diffraction condition and the effective medium approximation. That theory satisfactorily explained the angular and spectral positions of the resonant Wood's anomalies but was unable to describe the amplitude of the peaks as well as the entire reflection spectra. Moreover, the physical origin of the discussed Wood's anomalies in opals remained unclear.

The goal of the present work is to reveal the origin of the Wood's anomalies in the optical reflection of opals covered with high refractive index material $Ge_2Sb_2Te_5$ (GST225) [18]. For this purpose we perform the eigenmode analysis, simulate the reflection spectra, and calculate the electromagnetic near-field distribution in the opaline structures.

The structure of the paper is as follows. In Sec. II, we describe our hybrid GST225/opal structures, their fabrication technique, and the experimental setup. In Sec. II B, we give a brief description of the scattering matrix method and the way we approximate the structure to simulate our experimental results. In Sec. III, we present the results of reflection spectra
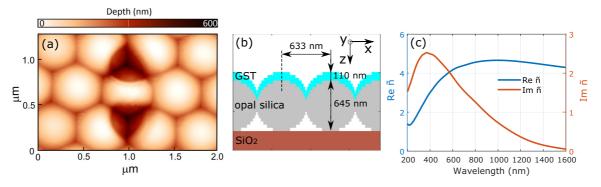
---
[*]s.dyakov@skoltech.ru

FIG. 1. (a) AFM image of a fragment of the GST225/opal structure where the GST225 film (light brown) is partially absent and SiO$_2$ spheres (dark brown) are exposed. (b) Schematic view of the structure used in scattering matrix method calculations. Only one monolayer of SiO$_2$ spheres is shown for simplicity. (c) Real and imaginary parts of the GST225 refractive index determined by ellipsometric measurements.

measurements as well as the results of numerical simulations. We analyze the angular dependencies of the Wood's anomalies and show how they relate to the dispersion relation of the quasiguided modes. We also calculate the electromagnetic near-field distribution of incident light. Finally, in Sec. IV we propose a simple model in order to describe the observed reflection spectra in terms of Lorentzian functions.

II. METHODS

A. Structure and experimental details

The samples of the hybrid structures under study consist of 1 and 16 monolayers of amorphous silica spheres of diameter ≈ 645 nm grown on fused silica substrate and covered by a GST225 film of ≈ 110 nm thickness [see Figs. 1(a) and 1(b)].

We determined the thicknesses of GST225 films deposited on opal by comparison with chalcogenide reference films deposited on a quartz substrate under the same technological conditions. The thicknesses of the reference films were measured with a profilometer. These values are in reasonable agreement with the atomic force microscopy (AFM) data presented in Fig. 1(a).

The fcc opaline lattice of spheres was grown from water suspension of amorphous SiO$_2$ particles by the vertical deposition technique [19]. The spread in diameter of spheres was smaller than 5%. The amorphous GST225 layer was deposited on the surface of opal films in vacuum by the thermal deposition technique at a substrate temperature of 50 °C, an evaporator temperature of 600 °C, and a residual pressure of 10^3 Pa (see Ref. [20]).

In optical measurements, the light of an incandescent lamp hits the structure at an incident angle θ changing from 11° to 66° with steps of 5°. The azimuthal orientation of the samples was set using the 2D optical diffraction pattern from the highly ordered (hexagonal) surface of the opal film. The following condition was satisfied: the incidence plane passed through one of the three equivalent pairs of sites of the hexagonal reciprocal lattice: (-11) (1-1); (01) (0-1); (-10) (10). The specular reflectance spectra were measured in the 900–1700 nm wavelength range with an Ocean Optics NIR 512 spectrometer equipped with an InGaAs-based charge-coupled device (CCD) array detector. Dependencies of the refractive index, Re $[\tilde{n}(\lambda)]$, and extinction coefficient, Im $[\tilde{n}(\lambda)]$, of the

GST225 films were determined with a J. A. Woollam Co., Inc., model M-2000 spectral ellipsometer.

B. Method of calculation

Currently many powerful theoretical methods are available to describe the optical properties of periodically modulated layers [21–27]. In this work the reflection spectra of hybrid structures are calculated using rigorous coupled wave analysis (RCWA) in the scattering matrix form [23–25]. This method is based on splitting a structure into elementary planar layers, homogeneous in the Z direction and 2D periodic in the X and Y directions. In this splitting, the circular cross section of each sphere is approximated by a staircase. The solutions of Maxwell's equations for each layer are found by expansion of the electric and magnetic fields into Floquet-Fourier modes (plane waves). The exact solution can be presented as an infinite series over these modes, in the limit of an infinite number of steps per sphere. In numerical simulations, the scattering matrices are determined by taking a finite number of stairs per sphere diameter, N_s, and by truncating the Fourier series on a finite number of plane waves N_p. The calculation accuracy increases with an increasing N_s and N_p; however, calculation time is proportional to N_s and N_p^3, respectively. In order to improve the convergence, we implemented Li's factorization rules [28]. As a result, we used 13 plane waves in both the X and Y directions so that the total number of plane waves was $N_g = 169$. The number of stairs per diameter was $N_s = 25$ in what follows. Our test calculations revealed that at these N_g and N_s the computation scheme numerically converges [29].

In addition, the choice of proper model of the geometry of the GST225 capping layer is an important issue. It will be seen later that a so-called crescent model adequately describes the influence of the capping layer on the reflection properties of the structures in this study.

The dispersion of the refractive index of GST225 is measured using the ellipsometry technique and takes the imaginary part into account [see Fig. 1(c)]. The refraction index of opal spheres is determined from the analysis of the Bragg reflection spectra of the initial opal film [denoted as opal silica in Fig. 1(b)] and is taken as 1.92, and is assumed to be independent of the wavelength [30].
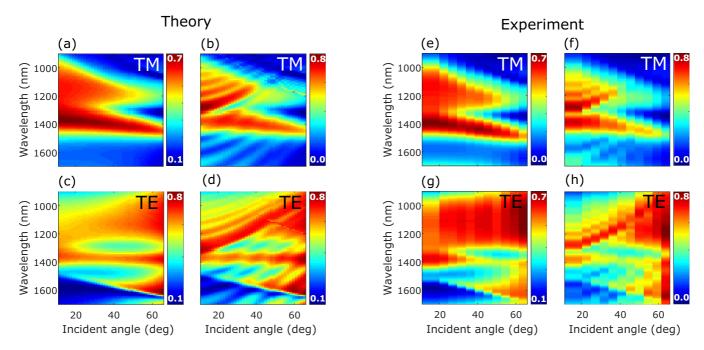
FIG. 2. Theoretical (left panel) and experimental (right panel) reflection of GST225/opal structure versus wavelength and incident angle in TM and TE polarizations. The reflection coefficients are shown for one monolayer of silica spheres [panels (a), (c), (e), and (g)] and for 16 monolayers of silica spheres [panels (b), (d), (f), and (h)]. The color scales are shown to the right of graphs. The thickness of the GST225 capping layer is $h = 110$ nm for all panels.

III. RESULTS

A. Reflection spectra

The theoretical and experimental reflection coefficients of the structures under study collected at different angles of incidence in TE and TM polarizations are shown in Fig. 2 as a two-dimensional function of photon energy and incident angle. In particular, Fig. 2(a) shows the theoretical reflection spectra of one monolayer of silica spheres covered by GST225 film. One can see that the spectra have two peaks which are redshifted with increase of the incident angle. In Ref. [17] these peaks were attributed qualitatively to the Wood's anomalies corresponding to two different quasiguided modes. At small enough angles θ the reflection spectra are strongly deformed and take an asymmetrical form, so that it becomes impossible to differ between separate peaks in the interaction region. The value of the reflection coefficient at peak positions (for the light

reflected in a small spatial angle) also monotonically increases with decreasing the angle θ, reaching its maximum at normal incidence ($\theta = 0$). At very small angles θ the Wood's anomalies merge into a broad irregular contour. A similar behavior is observed in TE polarization [see Figs. 2(c) and 2(d)].

The theoretical reflection spectra of the 16-monolayer hybrid structure show peaks of similar shape and the same spectral position [see Fig. 2(b)] along with the reflection maxima associated with photonic stop band and the Fabry-Pérot interference over the structure thickness. It is noteworthy that the theoretical and experimental spectra [see Figs. 2(e)–2(h)] are in a good agreement with each other.

In order to emphasize the influence of the GST225 film thickness, we calculated the reflection spectra of the structure without capping and with different capping thicknesses (see Fig. 3). The reflection of the structure without a capping layer does not show the Wood's anomaly described above [see
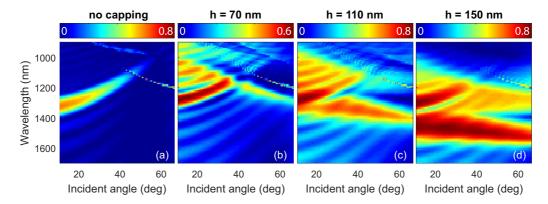

FIG. 3. Comparison of calculated reflection spectra of GST225/opal structure for various GST225 film thicknesses: $h = 0$, 70, 110, and 150 nm in panels (a), (b), (c), and (d), respectively. The color scales are shown on the top.
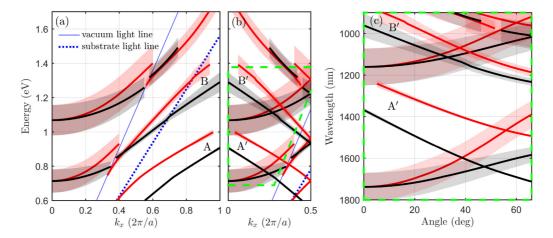
FIG. 4. (a) The calculated dispersion relations of eigenmodes of hybrid GST/opal structure in empty lattice approximation. GST225 film thickness is 110 nm. The red (black) color means the TM (TE) polarization. The width of red and black stripes in eV equals 1/3 of the imaginary part of the corresponding eigenenergy. The blue solid and dotted lines represent the vacuum and substrate light lines. The vertical dashed line denotes the boundary of the first Brillouin zone. (b) The dispersion folded in the first Brillouin zone. The dashed green line bounds the area which is represented in (c) in λ-θ coordinates.

Fig. 3(a)]. With increase of the GST film thickness, the Wood's peaks are redshifted while the photonic stop-band position and Fabry-Pérot resonances are practically not affected by GST225 film thickness. In addition to the photonic stop band and Wood's anomalies, the spectra in Figs. 3(a)–3(d) show sharp cusps which correspond to opening of the first diffraction channel (i.e., correspond to Wood-Rayleigh anomalies).

B. Dispersion of eigenmodes

The analysis of the reflection spectra made in the previous section suggests that the reflection peaks such as those in Fig. 2(a) are attributed to the interface layer of the hybrid structure. In order to reveal the origin of electromagnetic resonances in greater detail, the poles of the scattering matrix as a function of complex frequency ω and in-plane wavevector (k_x, k_y) have to be found [31–34]. The poles define the energy dispersion of the eigenmodes $\omega(k_x, k_y)$. Here $k_{x,y}$ are the x, y projections of the momentum vector of the incident wave. However, it appears that in this particular case the eigenmode dispersion can be found with a good accuracy from a simplified in-plane homogenized problem in the empty lattice approximation [25]. In this approximation, the dispersion relation is calculated for the new effective structure consisting of homogeneous isotropic layers corresponding to the consecutive steps of the staircase representation of the hybrid structure. The effective dielectric permittivities of these layers are calculated by the effective medium theory:

$$\varepsilon_{\text{eff}} = \frac{\sum_{\alpha} \varepsilon_{\alpha} f_{\alpha}}{\sum_{\alpha} f_{\alpha}}, \qquad (1)$$

where ε_{α} is the dielectric permittivity of αth component in a layer, and f_{α} is the filling factor of the αth component.

The approximate matrix S can be represented in the form of a 2×2 matrix. To account for the surface periodicity, the obtained dispersion curves are then folded back on the ω-k_x diagram into the first Brillouin zone.

The dispersion relations of eigenmodes of one monolayer of silica spheres covered by a 110 nm GST225 film are shown in Fig. 4. Figure 4(a) shows the dispersion curves of the effective nonperiodic structure. The modes above the vacuum light line are the Fabry-Pérot resonances. They have relatively large bandwidth (imaginary part of eigenfrequency) because of radiative losses due to the energy leakage to the far field. As to the modes below the substrate light cone (denoted as A and B), in the homogenized model they do not have radiative losses at all. Their nonzero imaginary part of the eigenfrequency is completely due to absorption losses in GST225 (In this respect, the homogenized model is valid provided that the radiative losses of modes A and B are smaller than the absorptive ones.). The modes A have longer lifetimes in comparison to the lifetimes of the modes B because the extinction coefficient of GST225, Im[$\tilde{n}$], at 0.9 eV is smaller than that at 1.35 eV [see Fig. 1(c)]. In Fig. 4, the stripes indicating the imaginary parts of eigenenergies of modes A are very narrow and are not visible to the naked eye.

Let us now account for the periodicity and fold the dispersion curves shown in Fig. 4(a) into the first Brillouin zone [see Fig. 4(b)]. The obtained eigenmodes A′ and B′ have now a negative dispersion. In order to compare the displayed dispersion curves with the experimental reflection spectra we plot the area bounded by the dashed green line in Fig. 4(b) in λ-θ coordinates [see Fig. 4(c)].

The comparison between the dispersion curves in Fig. 4(c) and the reflection spectra in Fig. 2(a) reveals that the TM reflection maxima at $\approx$1.4 eV and $\approx$1.2 eV are associated with the TM modes A and B. The other modes are not seen in the spectra as they have very large bandwidth. The correspondence between the reflection spectrum in TE polarization and the TE modes A and B is not very good. The reason for this is perhaps a stronger optical strength of the resonances, a stronger interaction between the quasiguided and Fabry-Pérot modes resulting in larger deviations from the empty lattice approximation [32].

The above analysis of the structure eigenmodes enables us to conclude that the reflection peaks shown in Fig. 2(a)
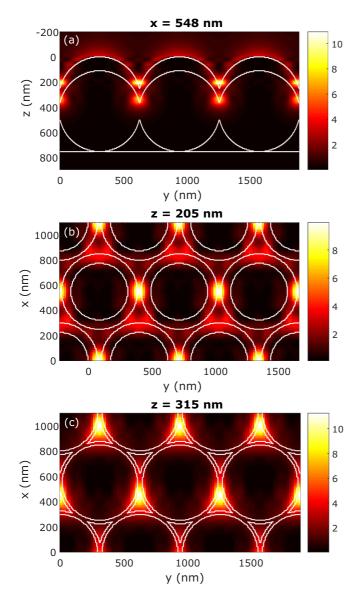
FIG. 5. Intensity of electric field of incident electromagnetic wave at $\lambda = 1310$ nm, $\theta = 56°$ in TM polarization calculated in displayed cross sections. White lines denote the interfaces between materials within the hybrid structure. Dashed horizontal lines in panel (a) show the positions of cross sections in panels (b) and (c). Electric field intensity is normalized to that of the incident plane wave. The color scales are shown on the right.

are associated with the resonant Wood's anomalies which correspond to quasiguided modes.

C. Field distributions

In order to visualize the modes described above, let us calculate the near-field distribution in the hybrid structures. We limit our discussion to the mode A, GST225 layer thickness $h = 110$ nm and TM polarization. The spatial distribution of the electric field intensity in the single-monolayer structure covered by the GST225 film is shown in Fig. 5 for $\lambda = 1310$ nm and $\theta = 56°$. This wavelength and angle of incidence correspond to the position of the dip in the reflection spectrum shown in Fig. 2(a). It can be seen in Fig. 5(a) that the
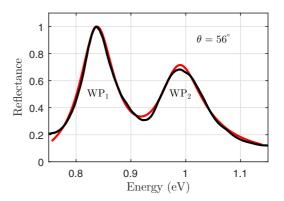

FIG. 6. The optical reflection spectrum (black line) for the hybrid photonic crystal (with GST film of thickness 110 nm) for the incidence angle $\theta = 56°$, which demonstrates the Wood's anomalies (WP$_1$ and WP$_2$) corresponding to two close quasiguided modes. The extrapolation of the spectrum is made by Eq. (2) (red line).

electric field is localized in the near-surface region and represents mostly a standing wave. In the antinodes, the field intensity reaches a maximum which is about 10 times higher than the field of the incoming wave. A field modulation coefficient, i.e., the ratio between the maximal and minimal electric field energies over the period of electromagnetic oscillation, exceeds unity by two orders of magnitude. This is also characteristic of the standing wave of the surface mode.

The spatial distributions of electric field calculated in two horizontal cross sections [marked by dashed horizontal lines in Fig. 5(a)] are shown in Figs. 5(b) and 5(c). It can be seen that the electric field is mainly localized in the gaps between the silica spheres.

IV. DISCUSSION

The analysis of the eigenmode dispersion curves and the electric near-field distributions reveals that the peaks in the reflection spectra are attributed to the appearance of the quasiguided modes [25]. Strictly speaking, these modes are the Fano resonances which are known to have an asymmetric line shape [35–37]. In our case, the asymmetry is weak and the reflection peaks can also be described in terms of a Lorentzian function. Figure 6 shows as an example the reflection spectra for the angle $\theta = 56°$ approximated by Lorentzian curves. Since the maximum of the peaks greatly exceeds the value of the reflection coefficient at some distance from the resonances ($\max[|r_j(\omega)|^2] \gg |r_{0j}|^2$, $j = 1,2$), this situation resembles the one seen in the case of the light reflection from a two-dimensional periodic array of objects demonstrating a resonant response in the absence of dielectric contrast, e.g., associated with excitons in isolated or tunnel-coupled quantum dots [38,39]. Relying on this analogy one can write the transmission coefficient for a hybrid structure as $t(\omega) = 1 + r(\omega)$, and taking into account the relation $|r|^2 + |t|^2 = 1$, one gets that $|r|^2 + \mathrm{Re}(r) = 0$. Further, the reflection coefficient can be presented as a sum of the pole terms $r = \sum_{j=1}^{N} r_j$, $r_j = f_j/(\omega_{0j} - \omega - i\Gamma_j)$, where ω_{0j} and $\Gamma_j = \Gamma_{0j}$ are the resonant frequency and radiative damping rate of the jth resonance. As a result,

one can obtain the following expression for the reflection coefficient:

$$R = |r|^2 = \sum_{j=1}^{N} \frac{\text{Im}(f_j)\Gamma_{0j} + \text{Re}(f_j)(\omega - \omega_{0j})}{(\omega - \omega_{0j})^2 + \Gamma_{0j}^2}.$$

By taking into consideration the absorption in the system, we can recast the last expression into the form

$$R(\omega) = \sum_{j=1}^{N} \frac{A_j + B_j(\omega - \omega_{0j})}{(\omega - \omega_{0j})^2 + \Gamma_j^2}, \qquad (2)$$

where A_j, B_j, and Γ_j are some real constants. Alternatively, Eq. (2) can be derived by considering a multipath interference from N resonances.

The extrapolation of the reflection spectra shown in Fig. 6 by Eq. (2), where the frequency ω is expressed in terms of energy ($\omega \rightarrow E[\text{eV}]$), gives the following fitting parameters: $A_1 = 0.058$, $B_1 = 0.077$, $\Gamma_1 = 0.039$ and $A_2 = 0.056$, $B_2 = 0.327$, $\Gamma_2 = 0.048$. Some discrepancy in the description of the experimental spectrum can be attributed to a difference of the spectral shape for the second mode of Wood's anomaly from the Lorentzian shape (due to a large broadening of the peak) and to the frequency dependence of the phase shift due to a difference in the spatial locations of the quasiguided modes in the near-surface region.

V. CONCLUSION

In conclusion, we have suggested a model of hybrid photonic crystal structure in which the vertical cross section of the GST225 capping layer has a crescent-like shape. It enables us to theoretically describe the Wood's anomalies in terms of the quasiguided modes which are localized in the gaps between silica spheres in the near-surface region. The measured reflection spectra of such structures are in a quantitative agreement with the simulation results obtained by the scattering matrix method. One can expect that the suggested model is sufficient for prediction of optical properties of other opal-based structures.

The potential practical applications of such structures include the development of promising elements for all-optical switches, filters, and multiplexers. Although the described resonances are in the near-infrared spectral region, the sensitivity of the reflection spectra to the GST225 capping layer paves the way for color management and light control.

[1] J. H. Holtz and S. A. Asher, Nature (London) **389**, 829 (1997).

[2] Y. Zhao, X. Zhao, J. Hu, M. Xu, W. Zhao, L. Sun, C. Zhu, H. Xu, and Z. Gu, Adv. Mater. **21**, 569 (2009).

[3] J. Grandidier, D. M. Callahan, J. N. Munday, and H. A. Atwater, Adv. Mater. **23**, 1272 (2011).

[4] R. B. Wehrspohn and J. Üpping, J. Opt. **14**, 024003 (2012).

[5] J. Üpping, A. Bielawny, R. B. Wehrspohn, T. Beckers, R. Carius, U. Rau, S. Fahr, C. Rockstuhl, F. Lederer, M. Kroll *et al.*, Adv. Mater. **23**, 3896 (2011).

[6] T. S. Shim, S.-H. Kim, J. Y. Sim, J.-M. Lim, and S.-M. Yang, Adv. Mater. **22**, 4494 (2010).

[7] S. Y. Lee, S.-H. Kim, H. Hwang, J. Y. Sim, and S.-M. Yang, Adv. Mater. **26**, 2391 (2014).

[8] D. Yang, S. Ye, and J. Ge, Adv. Funct. Mater. **24**, 3197 (2014).

[9] K. Ishizaki and S. Noda, Nature (London) **460**, 367 (2009).

[10] C. Tserkezis, N. Stefanou, G. Gantzounis, and N. Papanikolaou, Phys. Rev. B **84**, 115455 (2011).

[11] B. Ding, M. E. Pemble, A. V. Korovin, U. Peschel, and S. G. Romanov, Phys. Rev. B **82**, 035119 (2010).

[12] S. A. Dyakov, A. Baldycheva, T. S. Perova, G. V. Li, E. V. Astrova, N. A. Gippius, and S. G. Tikhodeev, Phys. Rev. B **86**, 115126 (2012).

[13] A. V. Korovin and S. G. Romanov, Phys. Rev. B **93**, 115440 (2016).

[14] K. I. Zaytsev and S. O. Yurchenko, Appl. Phys. Lett. **105**, 051902 (2014).

[15] S. Xiao, M. Qiu, Z. Ruan, and S. He, Appl. Phys. Lett. **85**, 4269 (2004).

[16] A. B. Pevtsov, D. A. Kurdyukov, V. G. Golubev, A. V. Akimov, A. A. Meluchev, A. V. Sel'kin, A. A. Kaplyanskii, D. R. Yakovlev, and M. Bayer, Phys. Rev. B **75**, 153101 (2007).

[17] M. M. Voronov, A. B. Pevtsov, S. A. Yakovlev, D. A. Kurdyukov, and V. G. Golubev, Phys. Rev. B **89**, 045302 (2014).

[18] S. Raoux, F. Xiong, M. Wuttig, and E. Pop, MRS Bull. **39**, 703 (2014).

[19] P. Jiang, J. Bertone, K. Hwang, and V. Colvin, Chem. Mater. **11**, 2132 (1999).

[20] S. Yakovlev, A. Pevtsov, P. Fomin, B. Melekh, E. Y. Trofimova, D. Kurdyukov, and V. Golubev, Tech. Phys. Lett. **38**, 768 (2012).

[21] M. I. Mishchenko, L. D. Travis, and A. A. Lacis, *Scattering, Absorption, and Emission of Light by Small Particles* (Cambridge University Press, Cambridge, 2002).

[22] F. J. García de Abajo and A. Howie, Phys. Rev. B **65**, 115418 (2002).

[23] M. Moharam, T. Gaylord, E. B. Grann, and D. A. Pommet, J. Opt. Soc. Am. A **12**, 1068 (1995).

[24] D. M. Whittaker and I. S. Culshaw, Phys. Rev. B **60**, 2610 (1999).

[25] S. G. Tikhodeev, A. L. Yablonskii, E. A. Muljarov, N. A. Gippius, and T. Ishihara, Phys. Rev. B **66**, 045102 (2002).

[26] K. Ohtaka and Y. Tanabe, J. Phys. Soc. Jpn. **65**, 2265 (1996).

[27] N. Stefanou, V. Yannopapas, and A. Modinos, Comput. Phys. Commun. **113**, 49 (1998).

[28] L. Li, J. Opt. Soc. Am. A **14**, 2758 (1997).

[29] See Supplemental Material at http://link.aps.org/supplemental/10.1103/PhysRevB.96.045426 for more details on the convergence of our numerical simulations.

[30] G. M. Gajiev, V. G. Golubev, D. A. Kurdyukov, A. V. Medvedev, A. B. Pevtsov, A. V. Sel'kin, and V. V. Travnikov, Phys. Rev. B **72**, 205115 (2005).

[31] N. A. Gippius, S. G. Tikhodeev, and T. Ishihara, Phys. Rev. B **72**, 045138 (2005).

[32] N. A. Gippius, T. Weiss, S. G. Tikhodeev, and H. Giessen, Opt. Express **18**, 7569 (2010).

[33] T. Weiss, N. A. Gippius, S. G. Tikhodeev, G. Granet, and H. Giessen, J. Opt. Soc. Am. A **28**, 238 (2011).

[34] D. A. Bykov and L. L. Doskolovich, J. Lightwave Technol. **31**, 793 (2013).

[35] U. Fano, J. Opt. Soc. Am. **31**, 213 (1941).

[36] U. Fano, Phys. Rev. **124**, 1866 (1961).

[37] B. Luk'yanchuk, N. I. Zheludev, S. A. Maier, N. J. Halas, P. Nordlander, H. Giessen, and C. T. Chong, Nat. Mat. **9**, 707 (2010).

[38] E. L. Ivchenko, Y. Fu, and M. Willander, Phys. Solid State **42**, 1756 (2000).

[39] M. M. Voronov and E. L. Ivchenko, Phys. Solid State **45**, 176 (2003).